

Active subsurface structures at Fayoum-Cairo district, Northern Western Desert, Egypt, as deduced from magnetic data

Ladislav BRIMICH¹, Ahmed KHALIL², Pavel KORDÍK³,
Mahmoud MEKKAWI², Mohamed EL-BOHOTY²,
Mohamed Khalil REFAI⁴, Abdou Khalaf Abdel KADER^{2,3}

¹ Geophysical Institute of the Slovak Academy of Sciences
Dúbravská cesta 9, 845 28 Bratislava, Slovak Republic; e-mail: geofbrim@savba.sk

² National Research Institute of Astronomy and Geophysics (NRIAG)
Helwan, Cairo, Egypt

³ Faculty of Information Technology, FIT, Czech Technical University
Thákurova 9, 180 00 Prague 6, Czech Republic; e-mail: rozvoj@fit.cvut.cz

⁴ Al-Azhar University, Faculty of Engineering, Cairo, Egypt

Abstract: In the present work, we present a reconnaissance study to elucidate and delineate the subsurface structures and tectonics of the area between Dahshour and El Fayoum province using available magnetic data; including land magnetic survey and aeromagnetic data. The study area has been selected due to its active tectonic situation. The magnetic data have been analyzed to provide new information about the tectonic setting and subsurface structures of the study area. A detailed land magnetic survey has been carried out for the total component of geomagnetic field using two Proton magnetometers, one of them as a local reading base station placed in the middle part of the area, while the second was used for measuring the total intensity of the different points in a mesh-like configuration. The necessary corrections for the measured magnetic data have been carried out. The total land intensity and aeromagnetic maps have been reduced to the north magnetic pole. Moreover, wave number filtering technique has been carried out on the magnetic data utilizing three types of filters with varying wavelengths. The application of these tools on magnetic data discriminated the variable sources of specific depth ranges for the residual and regional anomalies, as well as those limited to a certain depth interval. It was found that the main tectonic trends taken the directions NE–SW, NW–SE and E–W. Three basement cross-sections have been generated using the 2-D modeling to support the interpreted structures and give idea about the configuration of subsurface basement shape. Depth estimations have been conducted by application of the Power spectrum, analytical signal and 2-D modeling techniques. The results indicate that the average calculated depth ranges between 1.8 km to 3.5 km, while the depth to volcanic intrusions ranges between 0.20 km and 0.30 km.

Key words: land survey, aeromagnetic, subsurface structures and 2-D modeling

1. Introduction

The area under study is located in the northern part of Egypt between latitudes 28°30' and 30°00' N and longitudes 30°00' 32°00' E (Fig. 1). *Meshref et al. (1980)* analyzed magnetic trend in the northern part of Egypt and stated that the basement rocks in the western desert have been affected by two fault systems having large vertical and horizontal displacements. The oldest EW and ENE faults are intersected by the youngest NW and NNW. *Abu El-Ata (1990)* based on seismic and gravity data outlined three structural highs and two lows:

- a) Abu Roash high that strikes first NNE–SSW and then ENE–WSW.
- b) El-Sagha high which is oriented NW–SE.
- c) The El Faras-El Fayoum high that is oriented first ENE–WSW and then NNW–SSW.

Ghazala (2001) concluded that the four significant tectonic zones characterize the area of study, these zones are Nile Valley graben, East Nile Valley uplift, Ginidi basin and Kattaniya uplifl. The main aim of this study is to analyze the magnetic data and correlate them with the geological information, in order to define the significant fault patterns, which are responsible for the structural development of its geological units. To achieve this goal, various methods and techniques of analysis were applied to interpret the magnetic data of the study area.

The geological units of the study area started from Middle Eocene to the recent Nile sediments (*Naim et al., 1993* – Fig. 2). The structure of the area is dominated by faults, many of which can be identified from seismic and well data. The majorities are steep normal faults and most of them have a long history of growth, and some of the normal faults suffered strike slip movements during part of their history. Strike slip movements seem to have affected the orientation of many of the old fold axes. The strike slip movements were probably related to the lateral movements which the Africa plate underwent during the Jurassic and Late Cretaceous (*Said, 1990*). The area under investigation is structurally controlled by a set of normal faults having long periods of growth, and some of these faults show strike-slip movements. Deep drilling in the northern part of the Western Desert has shown a large number of swells and basins (*Said, 1990*). *Meshref et al. (1990)* state that

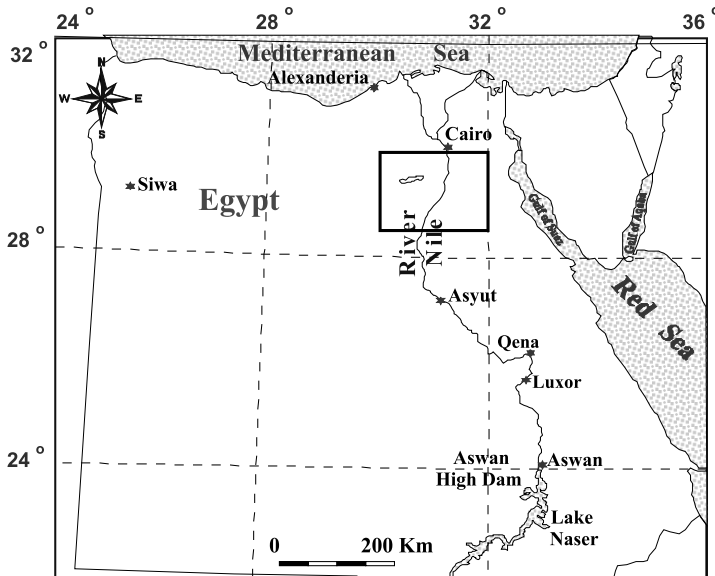


Fig. 1. Location map of the studied area.

the basement rocks in the Western Desert of Egypt have been affected by the oldest EW and ENE trending faults which in turn are intersected by younger NW and NNW trending faults. These two fault systems have large vertical and horizontal displacements. The area of Dahshour-Qattrani, in particular, is affected by the NW and EW trending faults. The NW trending fault, called the Qattrani fault, has a throw of about 350 m. However, the EW trending fault, called the G. Sheeb fault, has a throw between 150 and 200 m. The Oligocene basalt occupies these two faults.

2. Analysis of filtered magnetic maps

Five hundred land magnetic stations have been performed in the investigated area using the two Proton magnetometers of accuracy 1 nT. The first unit is fixed as a base station for the daily correction (diurnal variation), while the second unit is used for measuring the magnetic data at different station points. The interval between every two successive stations ranges

between 300 and 400 meters. GPS receivers have been used for locating the stations with accuracy of 1 m. The collected data are subjected to the two types of corrections; the first correction is performed to remove the effect of time variations on the measured magnetic data which is called diurnal variation correction. The second correction is completed by introducing the calibration factor of the two Proton magnetometers used in the measurements. The corrected magnetic data are plotted by using Geosoft program (*Oasis Montaj*, 1998) to represent the total intensity magnetic map (Fig. 3a). The total magnetic intensity is reduced to the north magnetic pole (RTP) using Geosoft program (*Oasis Montaj*, 1998) (Fig. 3b). The value of normal (IGRF11-2010) geomagnetic field for the study area is (F) – 43348.0 nT, declination (D) – 3.726°, inclination (I) – 44.339°, downward (Z) – 30295.9 nT and horizontal (H) – 31003.3 nT.

The processing of the total intensity land magnetic map (Fig. 3a) is started by reduction to the north magnetic pole (RTP), in which the RTP magnetic map is separated into residual and regional components. Their filters (regional, residual and band pass filters) and the least squares technique are used in the interpretation and delineation of shallow and deep

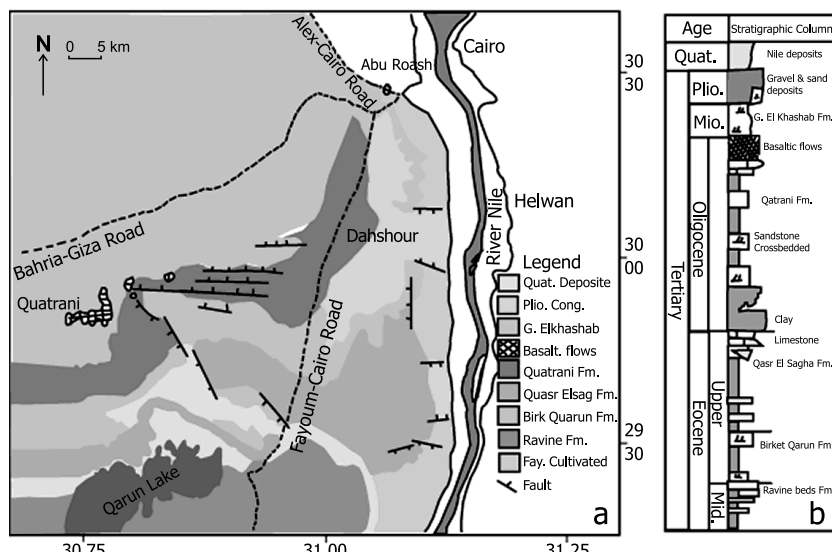


Fig. 2. Geological map of the studied area, NW desert, Egypt (after Naim et al., 1993).

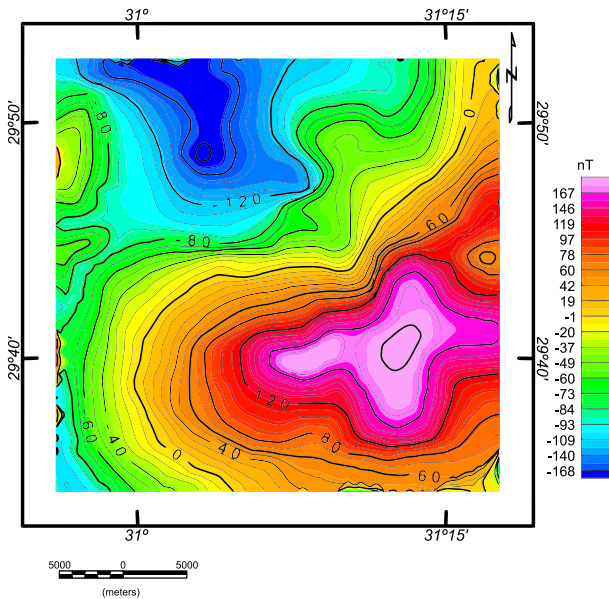


Fig. 3a. The total intensity land magnetic map of the studied area.

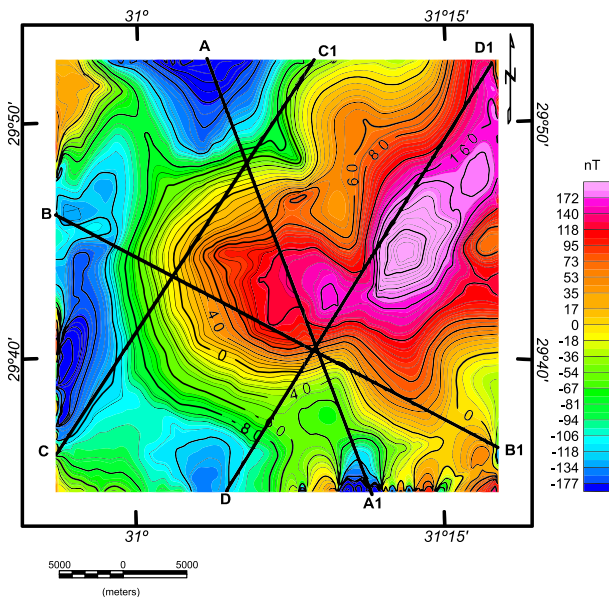


Fig. 3b. RTP land magnetic anomaly map of the studied area.

subsurface structures of the studied area. The quantitative interpretation has been used to determine the depths of shallow subsurface structures (faults and dykes), basaltic intrusions, as well as the basement complex of the considered area. The interpretation methods are the radially averaged power spectrum, Euler deconvolution, analytical signal and 2-D magnetic modeling. The processing and analysis have been done by a specialized computer software (*Geosoft V.4.3, 1993*). In order to overcome the undesired distortion of the shapes, sizes and locations of the magnetic anomalies, reduction of the total intensity land magnetic map to northern magnetic pole of the Earth has been applied. The resulting RTP land magnetic map (Fig. 3b) shows the direct correlation between the magnetic anomalies and their causative sources. The technique used in this transformation is that of *Baranov (1975)*. An average magnetic inclination 44° was used for the studied area, to eliminate the obliquity of the inclination of the Earth's magnetic field.

2.1. RTP land magnetic map

The inspection of the RTP land magnetic anomaly map of the studied area (Fig. 3b) reveals that the most striking criterion of the anomalies at Dahshour area is the NE–SW magnetic high. The main high is separated from a low by steep magnetic gradient with a shallow basement rocks. This steep gradient indicates that, the Dahshour area is structurally controlled by a fault having a major axis in NW–SE direction (Fig. 3b). Also, the area is characterized by intensive magnetic contour lines of positive values. This part reflects very strong magnetic anomalies with steep gradients and high amplitudes at the northeastern and southwestern sides. The strong magnetic anomalies may be attributed to the occurrence of subsurface basic intrusion of high magnetic content. The most conspicuous anomalous features of the northwestern platform, that has magnetic low (-40 nT) and extends in the NW–SE direction, are represented by incomplete negative magnetic anomalies of limited area extent and characterized mainly by their relatively low amplitudes, low frequencies and moderate gradient. These almost negative magnetic anomalies may be interpreted as structure lows or down-faulted basement blocks.

2.2. RTP aeromagnetic map

The total aeromagnetic map (Fig. 4a) has been reduced to the north magnetic pole as shown in Fig. 4b. The RTP aeromagnetic anomaly map (Fig. 4b) is characterized by the dominance of negative magnetic anomalies in the eastern and western parts. The central part is characterized by intense positive magnetic anomalies constituting several peaks. These peaks reflect very high magnetic susceptibility amplitudes. These anomalies may be attributed to the occurrence of subsurface basic intrusions of high magnetic content at different depths. Also, the differences in magnetic relief between each two adjacent magnetic highs and lows suggest a comparable variation of lithology. The map also shows the local magnetic anomalies superimposed on the regional magnetic field. These anomalies are most probably related to the basement faulting structure. Several intensive contours indicate the high horizontal magnetic gradients and could be interpreted as the locations of fault planes. Fault trees and axes as magnetic anomalies are trending in the N–S direction. The height of aeromagnetic survey is 140 m.

Filtering the magnetic maps is used to improve the understanding of the geological configuration of the basement and the overlying sedimentary cover. Therefore, the used filters are grouped into three categories, namely: regional (low-pass), residual (high-pass) and band-pass filters. The low-pass filter is defined as a filter which passes long wavelengths and rejects all wavelengths smaller than the cut-off wavelength. A high-pass filter emphasizes short wavelengths and eliminates wavelengths larger than the cut off wavelength. The high-pass magnetic filtered map with frequency cut off 0.080 cycle/km (Fig. 5b) contains a large number of smaller anomalies resulted from the filtering process. The residual magnetic filtered high-pass is more or less analogous to the residual magnetic filtered map (Fig. 6b) that separated by polynomial method, but with smaller number of anomalies and more gentle magnetic gradients. These anomalies are found to be distributed with varying trends. The prominent NW–SE and NE–SW anomalies trends in the central part were retained, but with shorter wave lengths than the original one. This indicates that the prominent fault trends are extended in the subsurface up to the shallow depths.

The low-pass filtering process is used to isolate the regional features from the local ones. The regional magnetic filtered map (Figs. 5a, 6a) shows that, the area is sub varying into three portions, the northern and southern lows

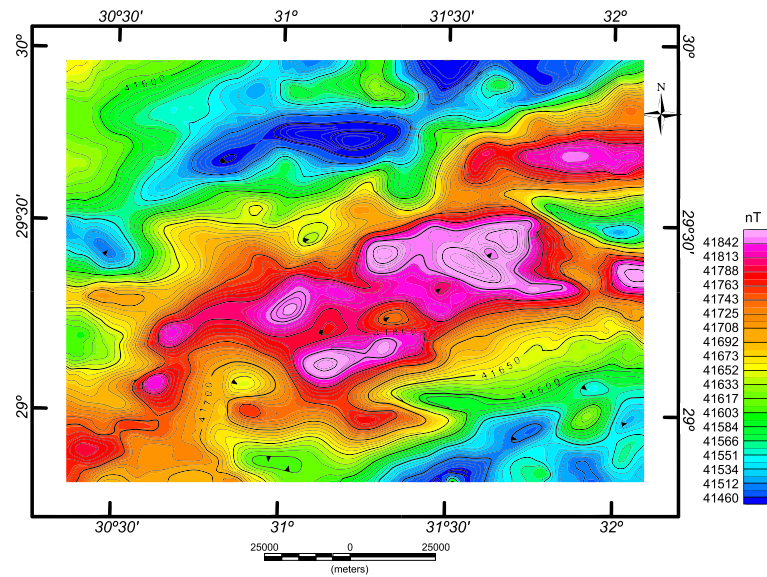


Fig. 4a. The total intensity aeromagnetic map of the studied area.

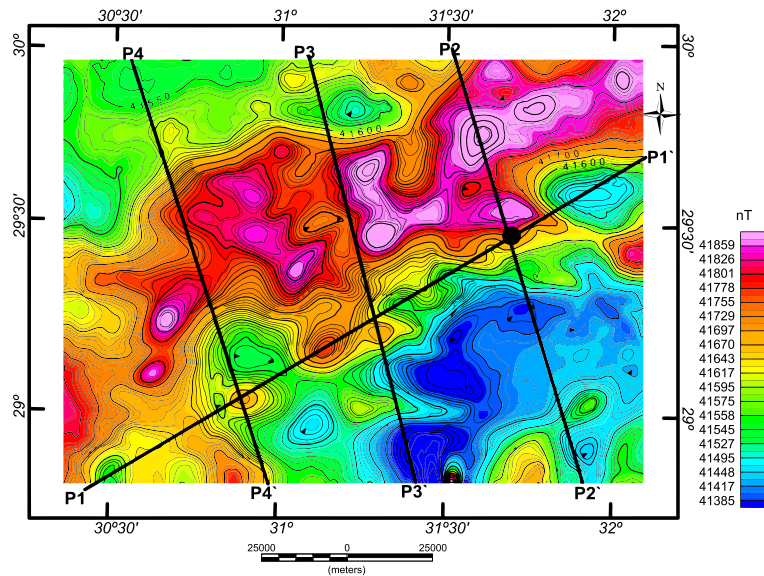


Fig. 4b. RTP aeromagnetic map of the studied area.

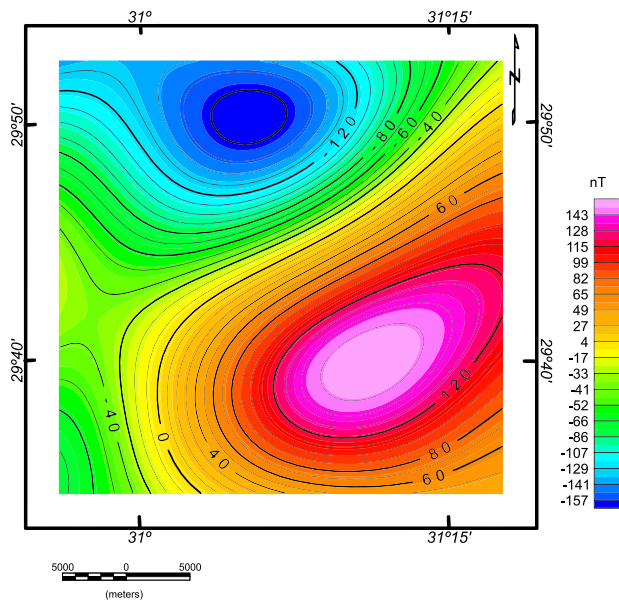


Fig. 5a. Low pass filter of the land magnetic data.

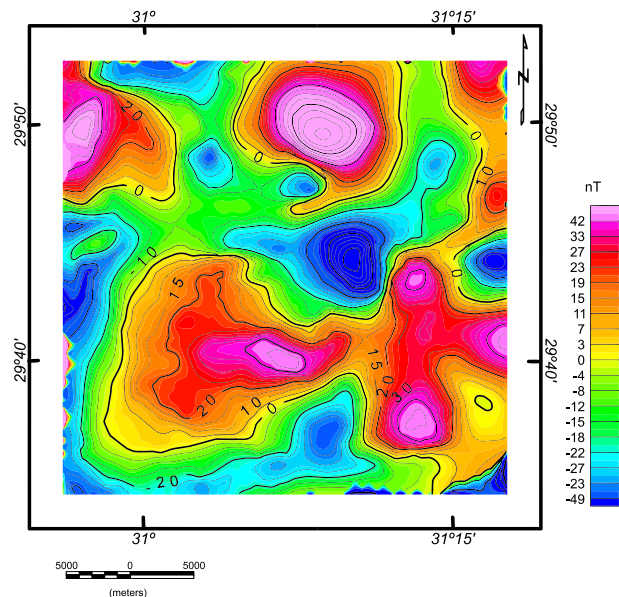


Fig. 5b. High pass filter of the land magnetic data.

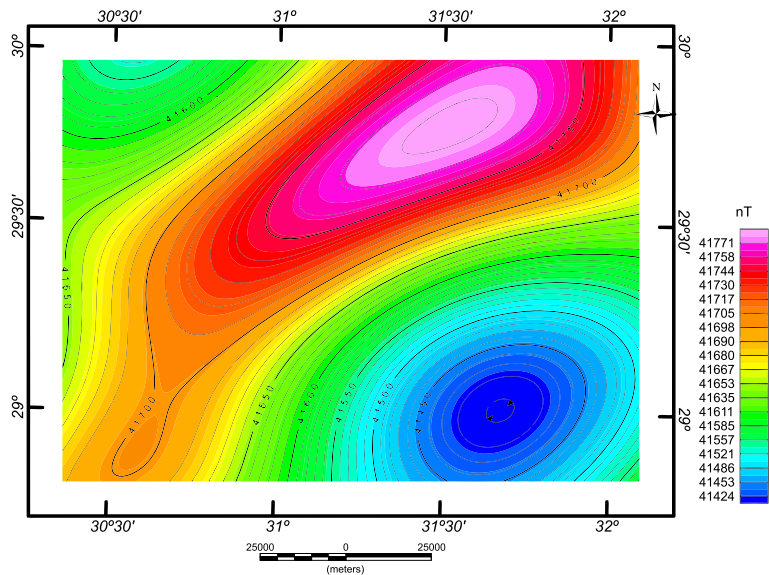


Fig. 6a. Low pass filter of the RTP aeromagnetic data.

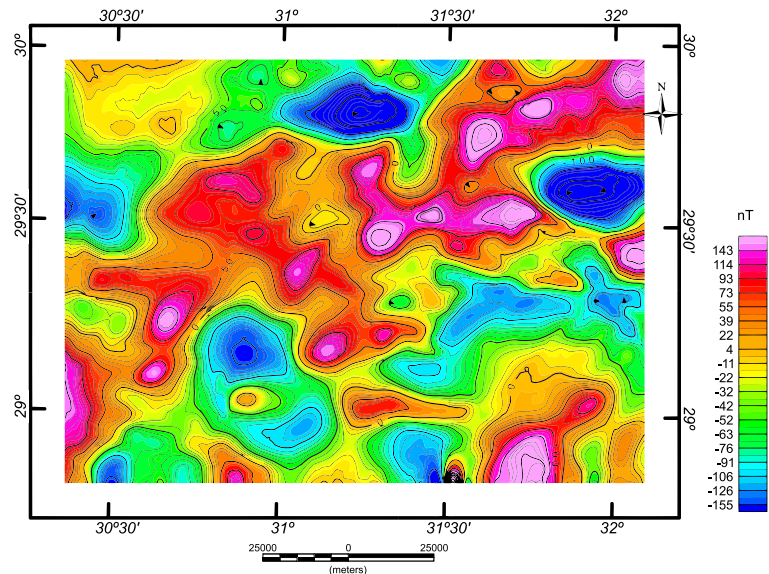


Fig. 6b. High pass filter of the RTP aeromagnetic data.

with negative anomalies and the central high positive one, these separated by steep gradients oriented NE–SW and NW–SE. Also we notice that, the well defined trends of anomalies in the aeromagnetic map are still persisted. This reflects the deep extension of the structures causing the anomalies.

3. Basement depth determination

The application of depth determination techniques, to identify the shapes of the causative geological bodies, is one of the most important parameters that must be outlined in order to interpret adequately the geology and structure of the area. Two techniques are used to calculate the depths of the causative bodies utilizing the magnetic data. These techniques are:

3.1. Euler deconvolution method

The Euler deconvolution method is a new tool used in interpretation of the potential field methods (gravity and magnetic), for determining the depths of the contact between the sedimentary rocks and basement rocks. This method depends on the structural index, level of the magnetic data and the sampling rate. This method uses both the horizontal and vertical gradients, to calculate the location and the depth of the anomaly sources. The Euler deconvolution technique is carried out on the magnetic data using *Geosoft program (1993)*. The depth to the subsurface structures ranges between 400 and 900 m. The Euler solution at different depths is shown in Figs. 7a, 7b. For interpreting contacts, faults and causative source type, for the magnetic data structural indices $SI = 1.0$ (for magnetic dykes) and $SI = 0.5$ (for magnetic fault) (*Riad et al., 1985*) are used. The depths to the detected faulting pictures off the subsurface structures range between 1.00 to 3.5 km with mean depth of 2.00 km.

3.2. Spectral frequency analysis

Radially averaged power spectrum method is used to determine the depths of volcanic intrusions, depths of the basement complex and the subsurface geological structures. Several authors, such as *Bhattacharya (1966)*, and

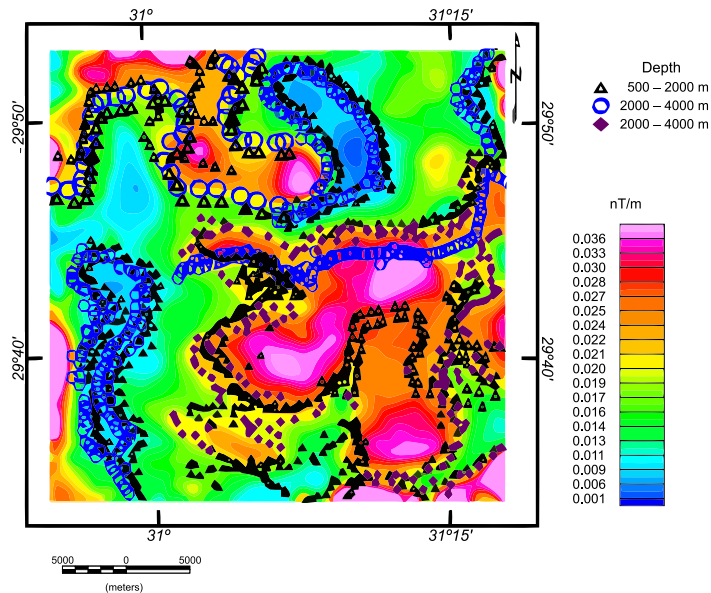


Fig. 7a. The Euler convolution for magnetic map of the studied area.

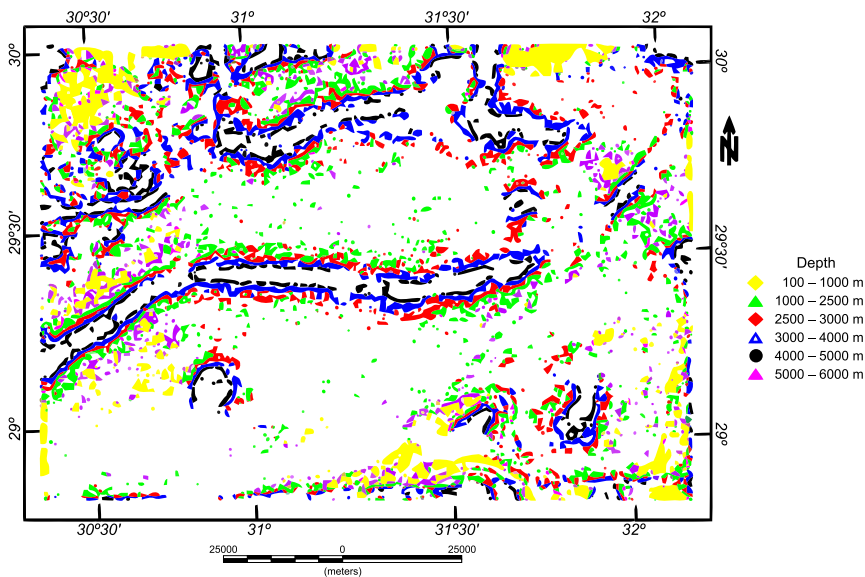


Fig. 7b. Euler convolution for aeromagnetic map of the studied area.

Spector and Grant (1970) explained the spectral analysis technique. It depends on the analysis of the magnetic data using the Fourier Transform. It is a function of wavelengths in both the X and Y directions. In the present study, the Fast Fourier Transform (FFT) is applied on the RTP aeromagnetic data and land magnetic survey data (Figs. 8a, 8b) to calculate the energy spectrum. As a result, a two-dimensional power spectrum curve has been obtained on which two main average levels (interfaces) at depth 0.5 km and 1.8 km below the measuring level (for the RTP aeromagnetic map) are revealed for the deep seated and near surface magnetic components respectively. On the other hand, the depth estimates of the land magnetic survey anomalies indicates that the depth of the basement complex lies at 1.8 km, while the depth of the basement intrusion is 0.4 km, below the measuring level.

4. Two-dimensional modeling of magnetic and aeromagnetic data

The two-dimensional modeling techniques of interpretation usually involve the fitting of geophysical parameters to potential data. Strictly speaking, potential modeling could be the inverse solution to a potential problem that cannot be done unambiguously. Theoretically, two reversed operations are performed sequentially, the first is a direct modeling process and the second is an inverse modeling process. The direct modeling process transforms the variations reflected by potential field data in an area of study, as shown by the residual potential anomaly mapping to a convenient subsurface geological setting. However, the inverse modeling process matches the calculated potential effects resulting from the inferred potential models with the observed one. With more geological control and well data, we can get information about the surface and subsurface magnetic susceptibility variations, established geological contacts and structural knowledge; the potential modeling can be performed with a higher degree of confidence. The computations of the magnetic effects for the assumed geologic models with complex geometry have been carried out with the aid of a computer program for the arbitrary two-dimensional polygon according to the method of *Talwani et al. (1959)*. *Hjelt (1974)* determined the criteria for making an adequate two-dimensional computation of various methods existing for calculation of

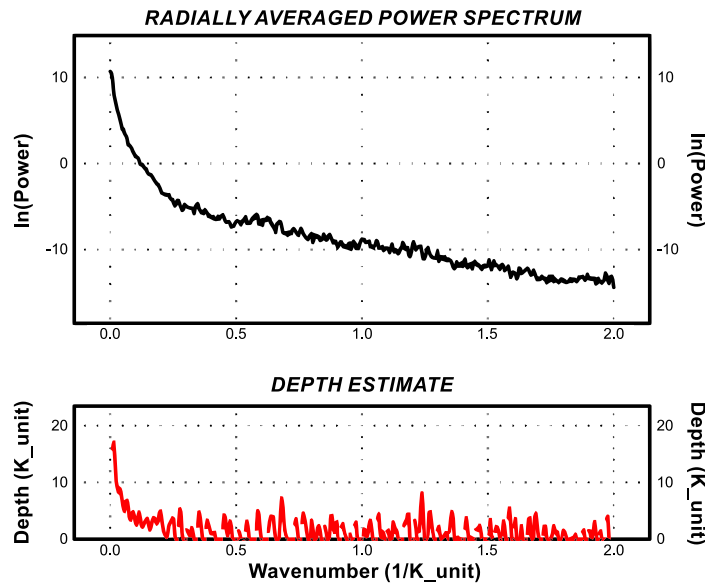


Fig. 8a. Radially averaged power spectrum of the magnetic data.

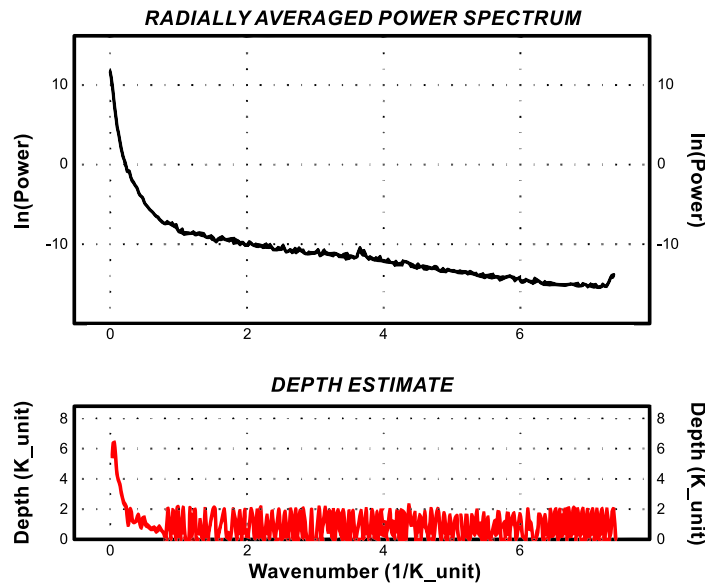


Fig. 8b. Radially averaged power spectrum of the aeromagnetic data.

the potential attraction caused by regularly and irregularly shaped bodies through profiles across two-dimensional bodies. It can be approximated through the use of charts (*Morgan and Faessler, 1977*), graticules (*Hammer and Anzoleaga, 1975*) or other similar graphical computation. Also, it can be computed analytically using the line-integral method (*Morgan and Grant, 1963*). Numerical computation of the line-integral is simplified for purposes of computer programming if the contour generating the lamina is represented by a polygon instead of a curved loop (*Dobrin and Savit, 1988*). For the present study, the line integral method has been used, and thus it will be discussed in some detail.

To confirm the interpreted magnetic basement structural framework of the study area, four regional magnetic profiles (Figs. 3b, 4b) were modeled using the 2D-forward modeling technique. The selected profiles were taken from RTP land magnetic map denoted as A-A1, B-B1 and from RTP aeromagnetic map denoted as P1-P1' and P3-P3' (Figs. 3b, 4b). The magnetic susceptibility contrast values for the sedimentary rocks and basement rocks along the four structural cross-sections were assumed. The magnetic field was calculated iteratively for these geological models, until a good fit was reached between the observed (dots) and calculated (line) profiles. The four models are shown in Figs. 9a, 9b, 10a and 10b. In these figures, the horizontal x-axis represents the horizontal distance in km along the profiles, while the vertical axis is the magnetic field scale in nT and the lower part represents the depth scale in km. The magnetic susceptibility of the basement rocks ranges between 0.004 and 0.005 S.I. units. The magnetic field responses computed for the geological models used the magnetic declination of 3.726° east and magnetic field inclination of 44.339°. The regional magnetic field intensity utilized was 42700 nT. From the investigation of the two-dimensional magnetic model, the profile A-A1 (Fig. 9a) lies in the central part of the area and is directed NW-SE. The basement is uplifted in the northern and central parts with a depth of about 1.2 km, and deepening in the southern part with a depth of about 2.5 km. From the profile B-B1 (Fig. 9b), it can be noticed that the eastern and western part is deeper than the central part. This means that the depth is increasing from the center toward the eastern and western side of the model. The basement is uplifted in the central part with a depth of about 2.5 km, while the depth in the deepest part of the model is about 3.5 km. Two dimensional magnetic

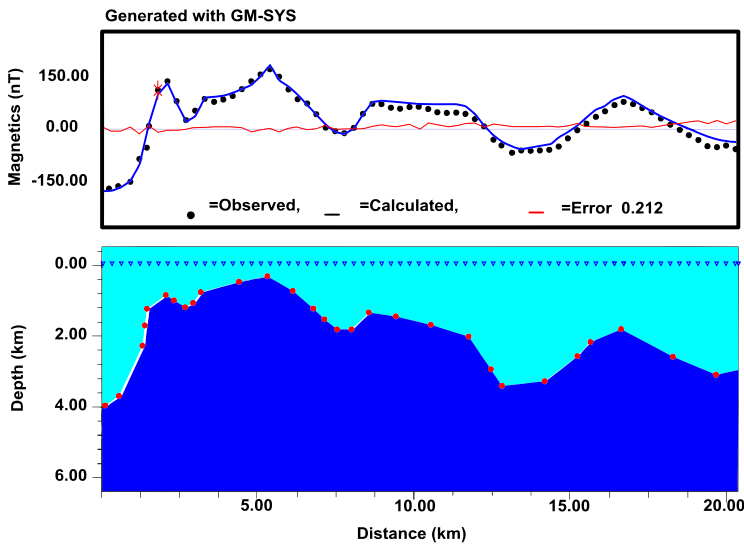


Fig. 9a. Two-dimensional modeling a long profile A–A1 of the RTP land magnetic anomaly map.

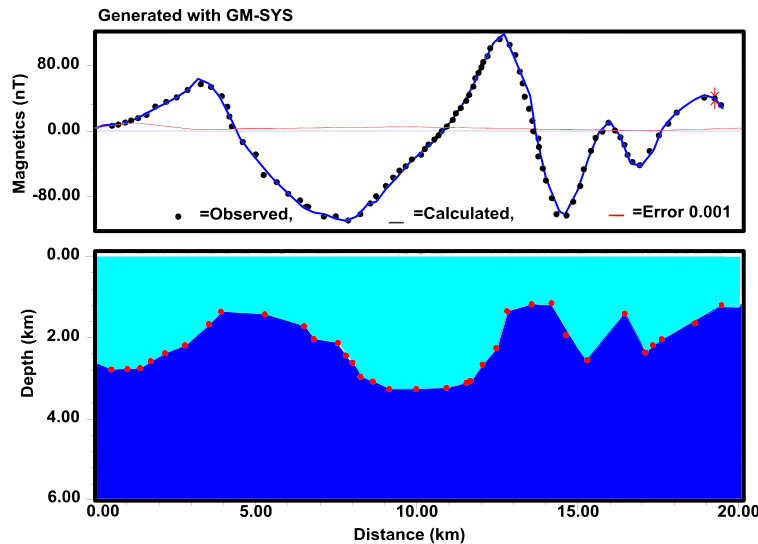


Fig. 9b. Two-dimensional modeling a long profile B–B1 of the RTP land magnetic anomaly map.

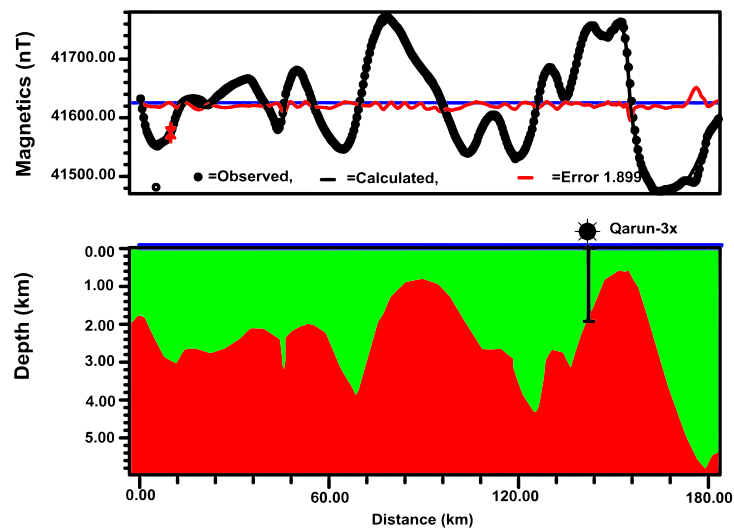


Fig. 10a. Two-dimensional modeling a long profile P1–P1' of the RTP aeromagnetic map.

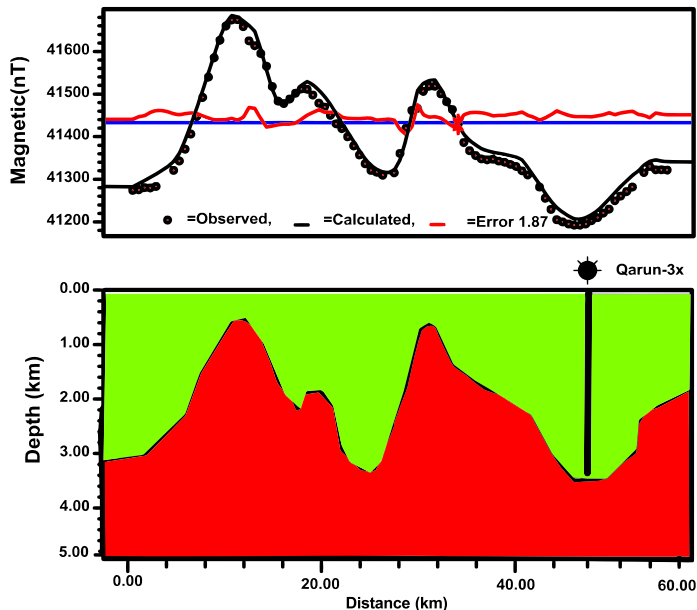


Fig. 10b. Two-dimensional modeling a long profile P3–P3' of the RTP aeromagnetic map.

models along the profile P-P' (Fig. 10a) lies in the central part of the area. The basement is uplifted in the northern part of the profile with a depth of about 1.8 km and deepening toward the southern part of the profile with the depth of about 4.1 km. The profile P3-P3' (Fig. 10b) lies in the north-eastern part of the area. The basement is uplifted near the northern part of the model, with a mean depth of about 3.8 km, and the general deepening toward the central part, with a basement depth of about 3.5 km.

5. Structural trend analysis

Geological interpretation of the potential field data is based mainly on deducing any relations between the available data and the subsurface structural conditions prevailing in the studied area. Structural trend analysis techniques have been frequently used in various fields of geology and geo-physics for the purpose of defining structural problems. *Hall (1964)* mentioned that there is a significant relation between direction, pattern and intensity of the magnetic anomaly trends. It can be attributed to the fact that the distinctness with which faults appear on the magnetic map depends principally on the existence and the strength of magnetic contrast in the body rocks involved. *Hall (1964)* discussed the significance of the anomaly peaks affecting the basement rocks as follows:

- A sharp peak with small standard deviation may indicate a trend caused by fracturing of uniform medium in response to stress of constant direction.
- A broad peak with large standard deviation may be expected to be formed by successive renewals of shifting stress direction.
- A peak with moderate symmetry may be formed by larger and smaller stress in different directions. The RTP aeromagnetic anomaly and the residual anomaly maps are interpreted to determine the common structural trends affecting the area of study. The azimuth and length of each detected lineament on the different maps represent probably the faults and/or contacts of varied lengths and directions.

These structure systems are statistically analyzed and plotted in the form of rose diagrams as shown in Fig. 11. The examination of these diagrams show

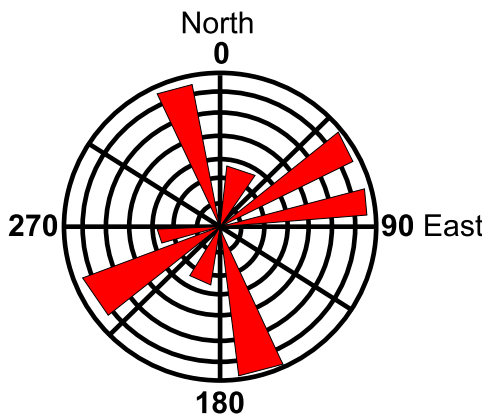


Fig. 11. Rose diagram shows analyzed and plotted structure trends systems in the study area.

three predominant structural trends having variable intensities and lengths. These are the NW, NE, and E–W trends, representing the most predominant tectonic trends affecting the investigated area as deduced from the magnetic point of view. However, the other minor structural trends appearing on the rose diagrams such as the N–S, NNE, and ENE are of less significance in this area. Each of the major trend category is described briefly in decreasing order, as shown below.

5.1. The NNW to SSE-trends

The correlation between the different rose diagrams reveals that the NW trend represents the most predominant trend direction in the studied area. This trend is referred to as the Eritrean or African trend (*Said, 1962*). He stated that it is cutting through the stable shelf in the most pronounced way and is of the greatest manifestation. It obviously occurred in the Mid-Tertiary time as it apparently related to the Red Sea and Gulf of Suez extent and direction as well as many other topographic features of the present day. *Mesherf et al. (1980)* stated that the NW-trend has a local magnetic distribution along the Red Sea coast and it fades away in areas at distances far from both sides of the Red Sea. However he did not explain the cause for this phenomenon. But *Mesherf (1990)* stated that the Western Desert of

Egypt shows a series of strong positive magnetic anomalies of the NW-trend as a result of the northward compressive force affecting the rocks of North Africa. However, *Neev* (1975) suggested that the NW trending tensional features were developed in the Red Sea region contemporaneously with the NE-trend fold system that were initiated due to the expansion of the central plate parallel to the Pelusium line.

5.2. The NE–SW trend

The NE–SW trend appears as the first major trend on the magnetic anomaly maps. The correlation between the rose diagrams of the observed and residual magnetic anomaly maps indicates that this trend has the same azimuth and intensity significance. Moreover, the NNE-trend appears as of trivial order on maps, suggesting and confirming that this trend is older than the NW and ENE-trends.

In such a manner, *Said* (1962) named this trend as Aqualitic trend, which was developed and related to the Gulf of Aqaba rift tectonics. He also mentioned that it was less pronounced around the stable shelf and bound many of the fold systems located in the middle part of Egypt (Syrian arc system). *Neev* (1975) stated that the Jordan-Dead Sea-Aqaba rift, which has been active as strike-slip fault since Oligocene time, has developed into a graben since late Pliocene time.

5.3. The ENE to WSW trend

This trend shows a great significance on the observed and residual magnetic anomaly maps. *Said* (1962) named this trend as a Tethyan trend that occurred during the Middle Cretaceous and seems to have continued more intensively during latter time. However, *Bayoumi* (1983) considered this trend to be caused by the second phase of tectonism prevailing from Early Mesozoic to Late Cenozoic. Also, *Ghazala* (2001) recorded this trend as a second and younger magnetic trend affecting the area just to the middle of the studied area. Therefore, it seems to be interpreted as one of the tectonic trend affecting the area of study that was initiated during the Precambrian time due to the eastward compressive stress and subsequently rejuvenated. Meanwhile, it occurs as a fault direction in the stable shelf and it is a

common basement direction in the exposed Pre-Cambrian basement rocks of Egypt.

6. Summary and conclusion

Our interpreted magnetic and aeromagnetic anomalies of the area between Dahshour and El Fayoum province have revealed a new information and improved the knowledge about the internal structure beneath this area. The present work is concerned with the determination of shallow and deep structures elements affecting both sedimentary section and the underlying basement complex in addition with quantifying the parameters of both basement complex and related volcanic basaltic intrusions at the study area using available magnetic data, including land magnetic survey and aeromagnetic data. Inspection of RTP land magnetic survey map (Fig. 3b) reveals that the map includes a wide elongated positive anomaly occupied the central part of the map and trending NE–SW. The observed relative difference in amplitude of magnetic anomalies recorded over this part may be related to either their lateral variation in lithology or in topographic relief, or both lithology and topography. The RTP aeromagnetic anomaly map (Fig. 4b) is characterized by the dominance of negative magnetic anomalies in the southeastern part of the study area. Also, the differences in magnetic relief between each two adjacent magnetic highs and lows suggest a comparable variation of composition of the subsurface rocks. The analysis of filtered maps indicate that the high pass magnetic filtered map characterized by prominent NW–SE and NE–SW anomalies trends in the central part. Also we notice that the well defined trends of anomalies in the aeromagnetic map are still persistent in the low magnetic-filtered map. This reflects the deep extension of the structures causing the anomalies. The Euler method is applied to the total field magnetic data. The application of these tools on magnetic data discriminated the variable sources of specific depth ranges for the residual and regional anomalies, as well as those limited to a certain depth interval. It was found that the main tectonic trends had the directions of NE–SW, NW–SE and E–W. Two basement cross sections are generated using the 2-D modeling to support the interpreted structures and give idea about the configuration of subsurface basement shape. Depth estimations are conducted by application of the power spectrum, analytical

signal and 2-D modeling techniques. The results show that the calculated average depth ranges between 1.8 km to 3.5 km while the depth to volcanic intrusions ranges between 0.20 km and 0.30 km.

Acknowledgments. Ladislav Brimich was partially supported by the VEGA grant agency under projects No. 2/0107/09 and 1/0461/09.

References

- Abu El-Ata A. S., 1990: The role of seismic-tectonics in establishing the structural foundation and saturation conditions of El-Ginidi basin, western Desert, Egypt. EGS (Egyptian Geophysical Society), Proc. of the 8th Ann. Meet, 150–189.
- Affleck J., 1963: Magnetic anomaly trend and spacing patterns. *Geophysics*, **28**, 379–395.
- Baranov V., 1975: Potential field and their transformation in applied geophysics. *Geo-exploration Monograph.*, Series L, 6, Gebruder Borntraeger, Berlin, Stuttgart, Germany.
- Bayoumi A. I., 1983: Tectonic origin of the Gulf of Suez, Egypt as deduced from gravity data, CRC. Hand book of geophysical explor. at Sea, 417–432.
- Bhattacharya B. K., 1966: Two-dimensional harmonic analysis as a tool for magnetic interpretation. *Geophysics*, **30**, 829–857.
- Cooper G. R. J., 1997: GravMap and PF proc software for filtering geophysical map data. *Computers and Geosciences*, **23**, 1, 91–101.
- Dobrin M. B., Savit C. H., 1988: Introduction to geophysical prospecting 4th Edn., McGraw Hill book company, New York.
- EGSMA (Egyptian Geologic Survey and Mining Authority), 2003: Geological map of Al-Fayoum quadrangle, Egypt, scale 1:250 000.
- Geosoft program v.4.3, 1993: Software for the Earth Science. Geosoft Inc., Toronto.
- Grant F. S., West G. F., 1965: Interpretation Theory in Applied Geophysics. McGraw-Hill, New York.
- Ghazala H., 2001: Tectonic setting of the area between Cairo and Fayoum provinces, Western Desert, Egypt: Implications of gravity models. Proc. 2nd the Intern. Symp. of Geophys. Tanta University, Egypt, 101–110.
- Hall D. H., 1964: Magnetic and tectonic regionalization in Texada island. *British Columbia Geophysics*, **29**, 4.
- Hammer S. S., Anzoleaga R., 1975: Exploration for stratigraphic Traps with gravity gradients. *Geophysics*, **40**, 256–268.
- Hjelt S. E., 1974: The gravity anomaly of a dipping prism. *Geoexplor.*, 2, 29–39.
- Meshref W., Abdel Baki S., Abdel Hady H., Soliman S., 1980: Magnetic trend analysis in the northern Arabian Nubian Shield and its tectonic implications. *Ann. Geol. Surv. Egypt*, **10**, 939–953.

- Meshref W., 1990: Tectonic Framework of Egypt. Edited by Said R., 113–156.
- Morgan A. N., Faessler C. W., 1977: A two and three-dimensional dot chart. *Geophys. Prosp.*, **20**, 363–374.
- Morgan A. N., Grant S. F., 1963: High-speed calculation of gravity and magnetic profiles across two-dimensional bodies having an arbitrary cross-section. *Geophys. Prosp.*, V, 11 p.
- Naim G., Hussein A., El-Hakim B., Sewidan A., 1993: A preliminary Report on the Dahshour earthquake, 12 October 1992. Egyptian Geological Survey, Internal report.
- Naim Gaber M., 1993: A Preliminary Report on the Dahshour Earthquake, 12 October 1992. Cairo, EGSMA.
- Neiv D., 1975: Tectonic evaluation of the Middle East and Levantine basin. Easternmost Mediterranean Geology, printed in U.S.A.
- Oasis Montaj, 1998: Geosoftmapping and application system. Inc., Suit 500 Richmond St. West Toronto, On Canada N5SIV6.
- Pelton C., 1987: A computer program for hill-shading topographic data sets. Computer and Geosciences, **13**, 5, 545–548.
- Riad S., El-Etr H. A., 1985: Bouguer anomalies and lithosphere-crustal thickness in Uganda. *Journal of Geodynamics*, **3**, 1-2, 169–186.
- Said R., 1962: The geology of Egypt. Elsevier publishing Company. Amsterdam, New York.
- Said R., 1990: The Geology of Egypt. Balkema Press, The Netherlands.
- Spector A., Grant F. S., 1970: Statistical models for interpreting aeromagnetic data. *Geophysics*, **35**, 293–302.
- Talwani M. J., Worzel I. M., Landisman M., 1959: Rapid gravity computation for two-dimensional bodies with application to the Mendocino Submarine fracture zone. *J. Geophys. Res.*, **64**, 49–50.